


Cite this: *Sustainable Food Technol.*,
2025, 3, 537

Synergistic antimicrobial effects of waste cotton cloth extracted cellulose with phytofabricated TiO₂ for potential application in agriculture

Chhavi Sharma,^{ab} Archana Rana,^{ab} Amit Kumar Kesharwani,^c Dinesh Singh,^{*c}
Ritu Srivastava^{ab} and Shailesh Narain Sharma^{ab}  ^{*d}

A substantial economic loss in agriculture due to plant microbial diseases has driven attention towards developing nanomaterials as antimicrobial agents for crop protection. The currently available fungicides and pesticides are highly toxic and non-degradable, causing environmental pollution and even being harmful to consumers of agricultural products. However, this work attempts to develop a non-toxic and biocompatible nanomaterial as a good antimicrobial agent. In this regard, a waste product, *i.e.*, waste or used cotton cloth, has been recycled and used as a source of cellulose (natural biopolymer) extraction and for isolation of nanocrystalline cellulose (NCell) as well. Another biocompatible nanomaterial, titanium oxide (TiO₂), was synthesized using *Azadirachta indica* leaf extract to utilize the advantage of phytochemicals in the green extract. Furthermore, the two eco-friendly nanocomposites of NCell were prepared as nanomedicines, one with commercially available chemical TiO₂ (CNC) and another with green TiO₂ (GNC). The nanocomposites (CNC and GNC), in comparison with their individual nanomaterials (NCell and TiO₂), were examined against phytopathogens: *Xanthomonas campestris* pv. *campestris* (Xcc), *Bacillus subtilis* (BS) and *Pseudomonas fluorescens* (Psfl); fungi: *Fusarium graminearum* and *Phytophthora* spp. The results illustrated the synergistic effects of NCell and TiO₂ as nanocomposites showing a stronger and longer ability to inhibit pathogen growth and, thus, proved GNC to be an excellent antimicrobial agent for crop protection in agriculture.

Received 16th June 2024
Accepted 30th November 2024

DOI: 10.1039/d4fb00182f

rsc.li/susfoodtech

Sustainability spotlight

The study on developing nanomaterials as antimicrobial agents for crop protection aligns well with the scope of sustainable food technology. This research focuses on sustainable agricultural practices by recycling waste cotton cloth to extract nanocrystalline cellulose (NCell) and synthesizing biocompatible titanium oxide (TiO₂) nanoparticles using *Azadirachta indica* leaf extract. These eco-friendly nanocomposites (CNC and GNC) demonstrated significant antimicrobial efficacy against various phytopathogens and fungi, highlighting their potential to replace toxic, non-degradable pesticides and fungicides. This innovative approach not only addresses environmental and health challenges associated with conventional agrochemicals but also contributes to the circular economy and sustainable intensification of food production.

1. Introduction

Agriculture suffers from significant losses globally due to microbial plant diseases caused by bacteria, fungi, and viruses. These pathogens threaten food security by reducing crop yield and quality.¹ Despite plants' natural defense mechanisms, harmful pathogens such as *Pseudomonas syringae*² and fungi such as *Fusarium* spp. and *Alternaria* spp. continue to cause

extensive damage. These fungi often produce toxic mycotoxins, endangering consumers and animals.³ The widespread use of synthetic fungicides and antimicrobials in agriculture has serious drawbacks, including toxicity, non-biodegradability, environmental pollution, and potential carcinogenic effects, necessitating the development of safer alternatives.

Nanotechnology offers innovative solutions for managing plant diseases sustainably. Metal oxide nanoparticles,^{4–8} including TiO₂, MgO, and ZnO, as well as graphene oxide,⁹ silver and gold nanoparticles,^{10,11} have demonstrated potent antimicrobial activity. For example, MgO nanoparticles combat soil-borne pathogens,¹² while TiO₂ nanoparticles inhibit microbial cells by generating reactive oxygen species (ROS). Silver nanoparticles (AgNPs) are examined as measures against the bacterium *Xanthomonas campestris* pv. *campestris* (Xcc).¹³ However,

^aCSIR-National Physical Laboratory, Dr K. S. Krishnan Marg, New Delhi-110012, India^bAcademy of Scientific & Innovative Research (AcSIR), Ghaziabad-201002, India^cDivision of Plant Pathology, ICAR-Indian Agricultural Research Institute, New Delhi-110012, India^dDepartment of Applied Physics, Delhi Technological University (DTU), Shahbad Daultpur, Main Bawana Road, Delhi-110042, India. E-mail: shaileshnarainsharma@dtu.ac.in

the high cost and potential environmental risks associated with silver and gold nanoparticles limit their application in agriculture. The present study addresses these challenges by developing cost-effective, eco-friendly nanocomposites using waste-derived cellulose and green-synthesized TiO₂ nanoparticles. Cellulose, a naturally abundant, biodegradable polymer, was extracted from waste cotton cloth and processed into nanocrystalline cellulose (NCC). NCC offers numerous benefits,^{14,15} such as a high surface area, excellent heat resistance, and functional groups (hydroxyl and carbonyl) that enhance antimicrobial properties. It has applications in various industries,^{16–18} including pharmaceuticals, food packaging, and textiles, and also has great prospects for biomedical applications such as drug delivery, antibacterial wound dressing, antimicrobial films, and photobacterial nanofillers for food packaging.^{19–22} The presence of a large number of chemical groups (hydroxyl or carbonyl) on its surface exhibits a high affinity towards various contaminants.²³ This property helps cellulose-based nanomaterials used for the adsorption of charged contaminants which attack the pathogen's surface to weaken or damage its cell wall. Incorporating another biocompatible nanomaterial²⁴ further amplifies these properties, creating nanocomposites with enhanced structural and functional capabilities to strengthen antimicrobial potency.

TiO₂ was chosen as another nanomaterial for its stability, biocompatibility, and antimicrobial potency.^{25–27} Notably, its photocatalytic properties produce ROS that damage bacterial and fungal cells,^{28–30} making it a promising material for plant disease control.^{31–33} The study employed a green synthesis method to produce TiO₂ nanoparticles using *Azadirachta indica* (neem) leaf extract,³⁴ known for its rich phytochemical composition. Neem has been valued for centuries for its antimicrobial, anti-inflammatory, and antioxidant properties, with over 300 bioactive compounds that enhance plant defense mechanisms. The nanocomposites were prepared by combining NCC with both green-synthesized and commercially available TiO₂ nanoparticles. The materials were characterized using advanced analytical techniques, including transmission electron microscopy (TEM), X-ray diffraction (XRD), and UV-Vis spectroscopy, to assess their structural and optical properties. These nanocomposites were then evaluated for their antimicrobial efficacy against key phytopathogens and beneficial microbes.

The primary bacterial pathogen tested was *Xanthomonas campestris* pv. *campestris* (Xcc), responsible for black rot in Brassicaceae crops^{35–37} such as cabbage, cauliflower, and broccoli. This disease causes V-shaped lesions on leaves, leading to significant yield losses. As per the reported literature,^{13,38–40} only silver, copper and chitosan nanoparticles have been demonstrated against Xcc. These NPs are either expensive or not eco-friendly. However, the nanomaterials explored in the present work are earth-abundant, cost-effective, non-toxic, and biocompatible. This work is a first attempt to prepare such nanomaterials with efficient antimicrobial strength against chosen antimicrobials, especially *Xanthomonas campestris* pv. *campestris* (Xcc). However, cellulose and TiO₂ have been explored for their antimicrobial action against different microbes but not against Xcc and other microbes explored in the present work. Moreover, only a few studies have reported

antimicrobial properties of nanocomposites of cellulose and TiO₂; one such report⁴¹ has demonstrated bacterial cellulose with CQD-TiO₂ nanocomposite action against *S. aureus* and *E. coli* bacteria only. The present work provides first-hand information on the reporting of microbicidal action of cellulose-TiO₂ nanocomposites against *Xanthomonas campestris* pv. *campestris* (Xcc) and other fungicides. Antifungal activity was assessed against *Fusarium graminearum* and *Phytophthora* spp., pathogens causing severe diseases such as *Fusarium* head blight in cereals (wheat and barley)^{42,43} and water- and soil-borne diseases in citrus,^{44,45} respectively. Both fungi are highly destructive, with *F. graminearum* producing mycotoxins such as deoxynivalenol, which poses risks to human and animal health. Additionally, the compatibility of the nanocomposites with beneficial biocontrol agents, *Bacillus subtilis* and *Pseudomonas fluorescens*, was also studied. These microbes play vital roles in suppressing plant diseases and enhancing soil health. *B. subtilis* manages bacterial wilt in tomatoes caused by *Ralstonia solanacearum*,^{46,47} while *P. fluorescens* protects seeds and roots from fungal infections.⁴⁸ The obtained antibacterial and antifungal results of nanocomposites were analyzed and compared with those of each other and their individual parent components. Thus, the present work aims to utilize the synergistic effect of TiO₂ and cellulose to increase their strength to damage bacterial cell growth without affecting the growth of biocontrol agents. Hence, the potential of prepared nanocomposites has been demonstrated for plant disease management or crop protection in agriculture.

2. Materials and methods

2.1 Materials used

Waste cotton cloth was picked from old daily used clothes. The 10% NaOH solution and 50% hydrogen peroxide used for the extraction process were purchased from Sigma-Aldrich. Acid treatment of extracted cellulose was done using concentrated sulphuric acid (98 wt%). The solvents used for washing and other testing purposes are DI water and absolute ethanol (99.9%). All the reactants and solvents used in the experiment were of analytical grade. The *Azadirachta indica* leaves were obtained from the ICAR-Indian Agricultural Research Institute campus. Titanium tetra isopropoxide (TTIP) with 99.99% purity was used as a precursor for the synthesis of green TiO₂, while commercially available titanium(IV) oxide (TiO₂) with 99.7% purity was used as chemical TiO₂ (C-TiO₂). TTIP and chemical TiO₂ were obtained from Merck Chemicals Limited. The bacterial strain *Xanthomonas campestris* pv. *campestris* (Xcc) Xcc-C7, *Bacillus subtilis* DTBS-5 (BS), and *Pseudomonas fluorescens* DTPF-3 (PSFL) were obtained from the bacteriology lab, Division of Plant Pathology, ICAR-Indian Agricultural Research Institute. The fungal pathogens *F. graminearum* and *Phytophthora* spp. were obtained from the ITCC department of ICAR-Indian Agricultural Research Institute.

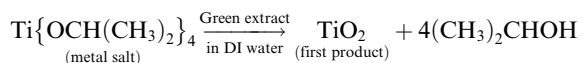
2.2 Synthesis

2.2.1 Cellulose extraction from cotton cloth. According to the extraction process,⁴⁹ waste cotton cloth, preferably white cotton



2.2.3 Preparation of *Azadirachta indica* leaf extract. 10 g of freshly finely chopped *Azadirachta indica* leaves were completely clean with deionized water and heated for 45 min with 50 ml of deionized water during constant stirring. The aqueous extract was filtered with Whatman filter paper no. 1 to eliminate any remaining impurities and kept at 4 °C for further use.

2.2.2.4 Green synthesis of TiO₂ nanoparticles. The titanium dioxide nanoparticles were synthesized using *Azadirachta indica* leaf extract and titanium tetra isopropoxide as a precursor. According to the procedure, 4 ml of titanium tetra isopropoxide precursor was added to 50 ml of green extract, and the solution was heated in a conical flask at 80 °C for 3 h with constant stirring. The phytochemicals found in leaf extract contribute to the conversion of metal salts to metal oxide nanoparticles and are also in charge of the reaction mixture's color change of particles. The color change from green to yellowish green confirmed the formation of nanoparticles. The reaction mixture was centrifuged at 5000 rpm for 15 minutes to separate the synthesized TiO₂ nanoparticles. The obtained sediment was dried in the oven overnight at 60 °C and further calcined at 400 °C for about 3 h in a furnace. The dried white powder obtained was the anatase form of TiO₂ nanoparticles which was stored in a glass bottle and marked as G-TiO₂. The anatase form of TiO₂ is known to be the most stable and highly non-toxic in nature with relatively low cost.



C for an hour to get the powdered nanocomposites marked as GNC (for G-TiO₂) and CNC (for C-TiO₂).

The synthesized nanoparticles' shape and size were analyzed using a transmission electron microscope (JEM 1011 model TEM). The well-sonicated ethanol dispersion of all the prepared nanomaterials was used to prepare carbon-coated copper TEM grids for testing. The absorption profile of all the samples was analyzed by UV-visible spectroscopy (Analytik Jena SPECORD 210 PLUS double beam UV-visible spectrophotometer). The diffraction pattern showing the phase composition of the nanocomposites in comparison with their parent components was analyzed by using a powder X-ray diffractometer (XRD) using CuK_α radiation of wavelength ($\lambda = 1.5418 \text{ \AA}$) in the range of $2\theta = 20^\circ$ to 80° with a scan rate of $0.02 \text{ deg per second}$. Each measurement of XRD was recorded using $\sim 50 \text{ mg}$ of well dried powdered sample. The data obtained from XRD and UV-visible spectroscopy were plotted using Origin software.

2.4.1 Bacterial culture. All the bacterial strains (Xcc, BS and Psfl) were cultured in nutrient broth (NB) (SRL, India) for 24–48 h at 28 °C with 200 rpm in a rotary shaker. The optical density of bacterial culture was measured using a spectrophotometer (Thermo Fisher Scientific, USA) at a 600 nm wavelength and maintained at a 0.5 McFarland unit – 1.5×10^8 cfu ml⁻¹.

2.4.2 Antibacterial activity. The antibacterial activity of nanomaterials (NPs and nanocomposite NC) was evaluated using the agar well diffusion method^{18,50,51} against *X. campestris* pv. *campestris*, *B. subtilis* and *Pseudomonas fluorescens*. Nutrient Agar (NA) plates were prepared by spreading 100 μ l of 1.5×10^8 cfu ml⁻¹ bacterial suspension evenly over solidified nutrient agar. Then, a well of 5 mm was punctured in these bacterial NA plates, and 50 μ l of nanomaterial to be tested was poured into the well. The prepared plates were kept at 28 °C for 48 to 72 h in an incubator. The inhibition zone (IZ) was observed at 48 and 72 h of incubation. The experiment was conducted at different concentrations (2, 4 and 8 mg ml⁻¹) of nanomaterials, and the results mentioned here present the optimized concentration. Each concentration has been tested thrice, and the results were repeatedly the same with an uncertainty of ± 1 mm IZ.

2.4.3 Antifungal activity. The poison food agar assay has been used to evaluate the nanomaterials' antifungal activity against mycopathogens – *F. graminearum* and *Phytophthora* spp. Potato dextrose agar (PDA) medium plates were prepared and supplemented with different concentrations (4, 2, 1, 0.5, 0.25 and 0.125 mg ml⁻¹) of the samples. A small plug of 3-day mycelial growth of *F. graminearum* and *Phytophthora* spp. was placed on the prepared PDA plates and incubated at 28 °C for 5 days. The results were observed after 5 days of incubation.

3. Results and discussion

3.1 X-ray diffraction pattern analysis

The diffraction peaks recorded using XRD spectra (shown in Fig. 1) represent the crystalline phases of the prepared

nanocomposites (CNC and GNC) as compared with their individual components (NCell and TiO₂), reflecting their joint contributions in composites. The characteristic peaks of TiO₂ (both chemical and green synthesized) are indexed according to the JCPDS card no. 21-1272, which reflects the pure anatase phase.⁵² On the other hand, the XRD spectra of nanocrystalline cellulose featured three characteristic peaks with $2\theta = 16.4^\circ$, 22.5° , 34.5° corresponding to (110), (200) and (004) planes, respectively.^{53–55} However, the characteristic peak of NCell corresponds to the (200) plane, and XRD peaks of TiO₂ correspond to (101), (004), (200), (105), (211), and (204) planes simultaneously featured in XRD spectra of nanocomposites (CNC and GNC). This confirms the successful formation of nanocomposites featuring the contribution of both NCell and TiO₂.

The X-ray diffraction pattern has also been used to determine the crystallite size in a solid by using the Debye Scherrer equation.^{56,57}

$$D = K\lambda/\beta \cos \theta$$

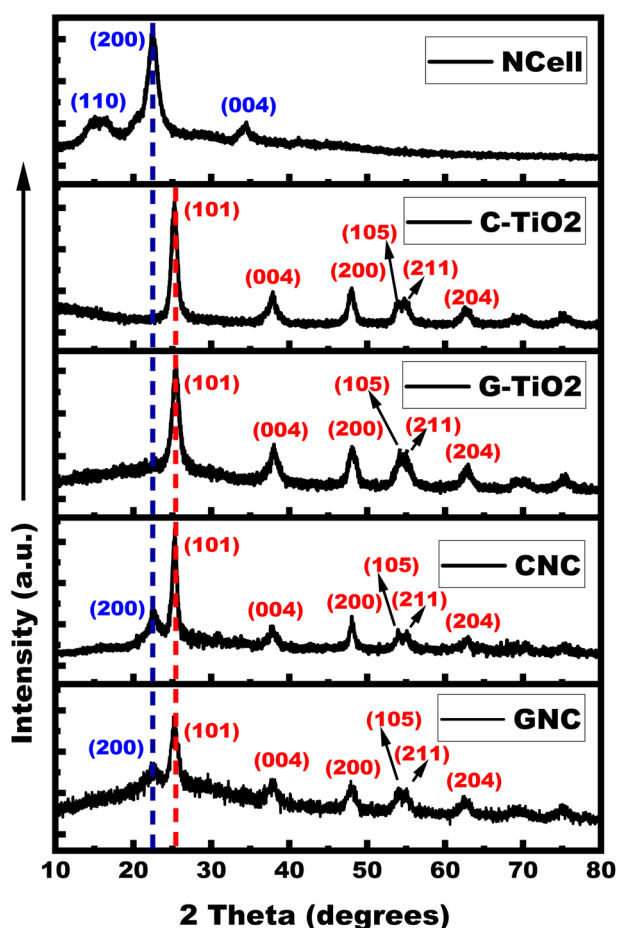


Fig. 1 X-ray diffraction pattern of nanocrystalline cellulose (NCell), C-TiO₂ (chemical TiO₂), G-TiO₂ (green synthesized TiO₂), CNC (NCell : C-TiO₂ nanocomposite) and GNC (NCell : G-TiO₂ nanocomposite).

where D = crystalline size of the nanoparticle. K = Scherrer constant equals 0.98. λ = Wavelength of X-rays (1.54 \AA). β = Full width at half maxima.

The calculated value of crystallite size of nanomaterials has been recorded and is shown in Table 1.

3.2 Optical characteristics

The absorption spectra shown in Fig. 2 have been obtained using UV-visible spectroscopy for optical analysis. It can be clearly seen that cellulose and TiO₂ both exhibit absorption in the ultraviolet region. Considering that the slope of the absorption band corresponds to the absorption edge of a material, the NCell absorption is slightly blue-shifted compared to that of CCell. Similarly, the C-TiO₂ absorption peak is blue-shifted compared to that of G-TiO₂. This blue shift in the absorption profile suggests particle size reduction. However, the absorption spectra of the nanocomposite showed the characteristic features of both NCell and TiO₂. This suggests the contribution of both individual parent components to the optical properties of nanocomposites, similar to the inference obtained from XRD spectra.

3.3 Structural and morphological analysis

The particle shape and size of prepared materials were analysed using TEM images shown in Fig. 3. Image (a) depicts the cluster of long fibers of cellulose extracted from waste cotton cloth while nanocrystalline cellulose (NCell shown in image b) isolated from extracted microcrystalline cellulose shows spherical nanoparticles of size $\sim 35\text{--}50 \text{ nm}$. Images (c) and (d) exhibit commercial TiO₂ of particle size $\sim 20 \text{ nm}$ and green synthesized TiO₂ with particle size $\sim 20\text{--}25 \text{ nm}$, respectively. Thus, the particle size of C-TiO₂ is found to be lower as compared to G-TiO₂, commensurating well with the UV-visible absorption results. However, images (e) and (f) belong to the nanocomposites of NCell with commercial chemical TiO₂ (CNC) and green synthesized TiO₂ (GNC), respectively. The TEM image of CNC depicts spherical nanoparticles of size $\sim 16\text{--}20 \text{ nm}$, while that of GNC depicts $\sim 7\text{--}12 \text{ nm}$ spherical nanoparticles. Moreover, particle agglomeration is noted in the CNC image, while the GNC image depicts evenly distributed nanoparticles. Hence, the TEM results suggest that the nanocrystalline cellulose nanocomposite with green synthesized TiO₂ exhibits better morphology than the nanocomposite of chemical TiO₂, as GNC shows good particle distribution with lower or no agglomeration. This indicates that the phytochemical-rich green extract in

Table 1 The crystallite size of all the samples calculated by using the Debye Scherrer equation

Sample	β	2θ	D (nm)
NCell	0.3	22.42	28.18
C-TiO ₂	0.38	25.23	21.25
G-TiO ₂	0.4	25.28	22.37
CNC	0.52	25.32	16.35
GNC	0.72	25.44	11.81

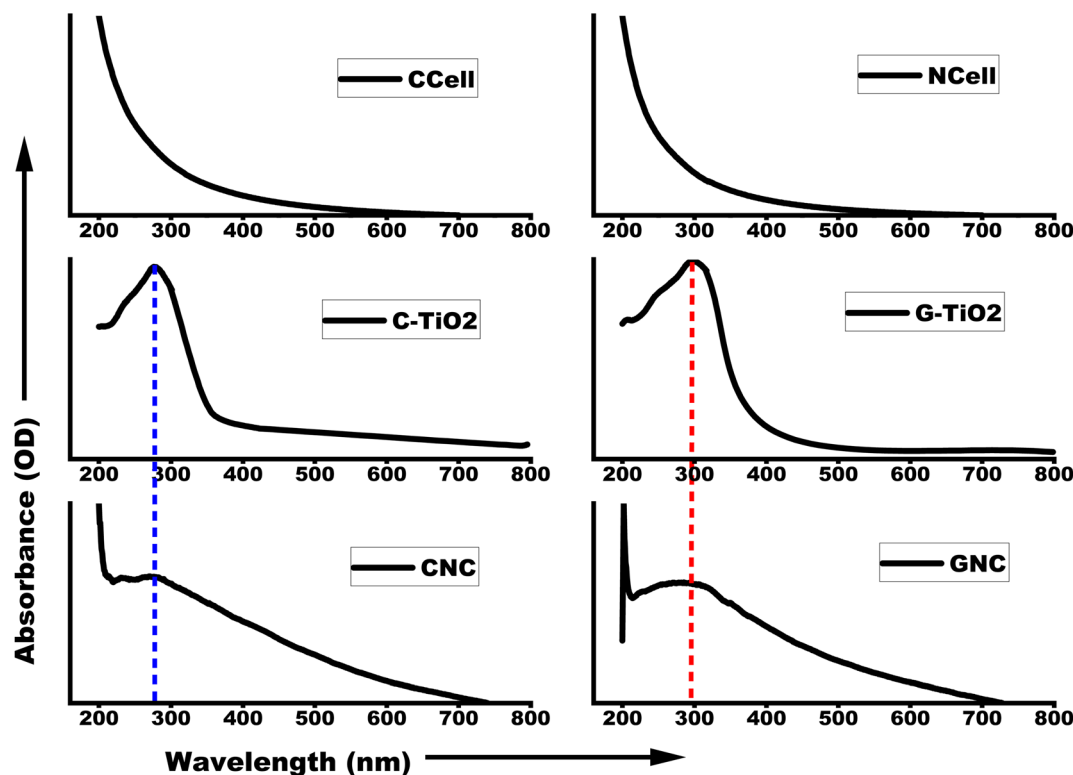


Fig. 2 Absorption profile of cotton extracted cellulose (CCell), nanocrystalline cellulose (NCell), C-TiO₂ (chemical TiO₂), G-TiO₂ (green synthesized TiO₂), CNC (NCell: C-TiO₂ nanocomposite) and GNC (NCell: G-TiO₂ nanocomposite) obtained from UV-visible spectroscopy.

the TiO₂ material played an important role in the preparation of nanocomposites. Moreover, the results obtained from TEM commensurate well with the crystallite size calculated using X-ray diffraction patterns.

Furthermore, the particle size distribution has been analyzed by using dynamic light scattering. Although DLS is too sensitive toward the presence of even small aggregates as I (scattering intensity) $\propto R^6$ (particle radius), it is used to determine the size distribution profile of particles in a suspension, measuring the hydrodynamic size of particles. Thus, it provides the nanoparticle size much larger than that analyzed using TEM results. Therefore, DLS data owe to hydrodynamic diameters based on ligands, ionic species, capping agents, solvents, etc. However, it can be appropriately utilized to monitor the PDI (polydispersity index) value to determine its monodispersity/polydispersity nature. The PDI value represents the particle size distribution, which should ideally be less than 1 to show monodispersity. Table 2 presents the particle hydrodynamic size of all the samples along with their PDI values. It has been found that the PDI value of all the samples is less than 1 owing to their monodispersive nature. Fig. 4 describes the particle size distribution of all the synthesized nanomaterials, while the inset figure shows the plot of the DLS correlation coefficient *versus* time. The particle size distribution profile shows a broad peak of chemical TiO₂ while the sharpest peak of the phyto-fabricated nanocomposite *i.e.*, GNC. Similarly, the correlation decay of GNC is steeper than that of all other samples, and its PDI value (0.2) is also lower comparatively, which indicates that

it is more stable or monodispersive than other nanomaterials. Thus, the DLS analysis also makes evident that the phytofabricated nanocomposite is the most stable and monodispersive nanomaterial.

3.4 Antibacterial study of synthesized nanomaterials

The antibacterial properties of nanocomposites (CNC and GNC) in comparison with their parent components (NCell, chemical TiO₂ and green TiO₂) were analyzed by the agar well diffusion method at different concentrations (2, 4 and 8 mg ml⁻¹). Initially, the experiment was conducted at an 8 mg ml⁻¹ concentration, but all the nanomaterials showed no activity at this concentration. It might be the case that the density of nanoparticles is too high, providing higher chances for agglomeration, due to which the nanoparticles could no longer maintain smaller particle size. Since particle size is one of the major factors responsible for the defensive mechanism against pathogens, small particles comparatively have a high ability to rupture and penetrate the bacterial cell wall.^{58–60} Keeping this in mind, the concentration of the nanomaterials has been reduced to 4 mg ml⁻¹ and tested against phytopathogen *X. campestris* pv. *campestris*, and the results were observed until 72 h, as shown in Fig. 5. Furthermore, the concentration of all the nanomaterials was reduced to 2 mg ml⁻¹ and expected to provide better results but found no reactivity of nanomaterials against phytopathogen. This suggests that the density of NPs at lower concentrations (2 mg ml⁻¹) is so low that the collective strength of NPs



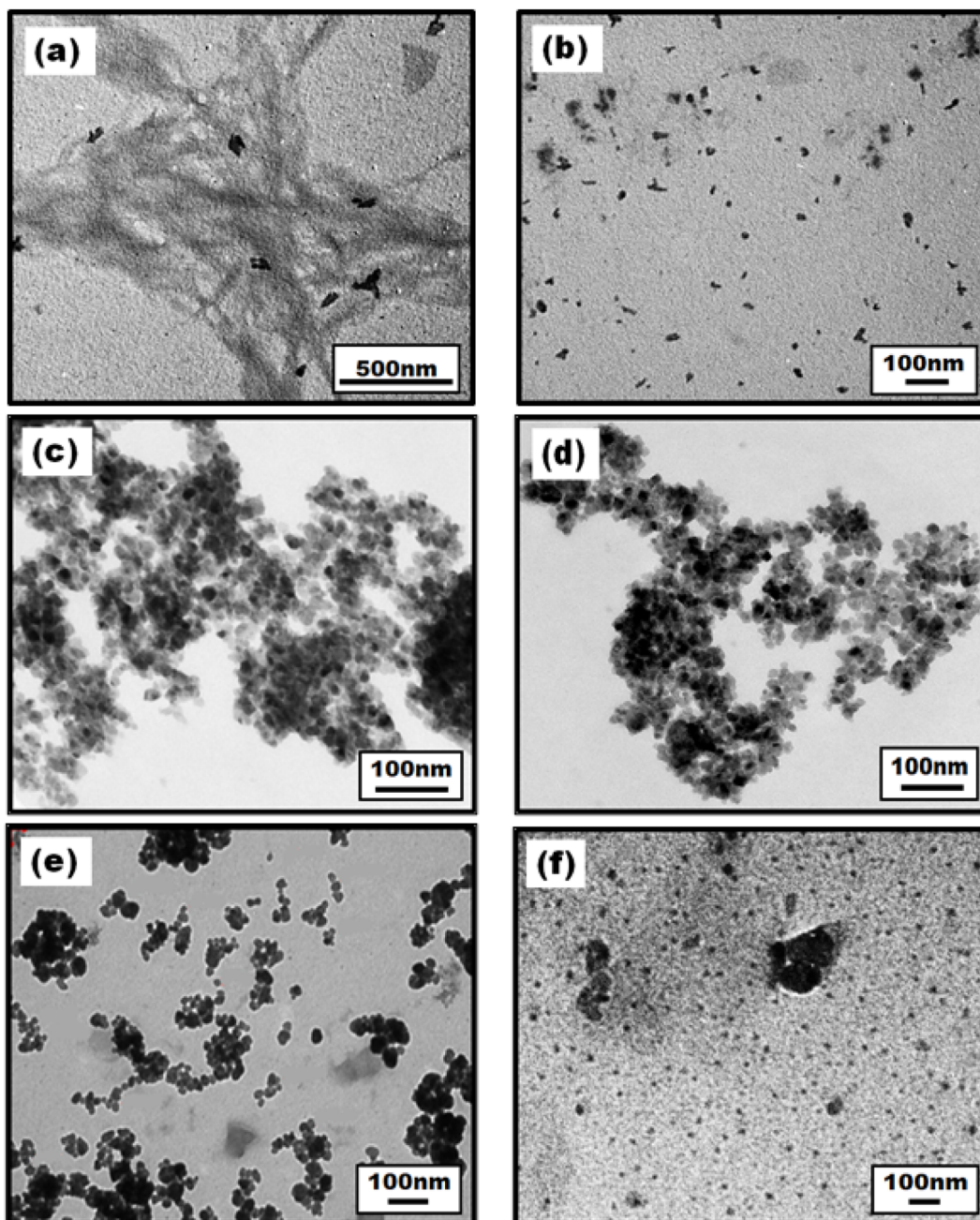


Fig. 3 Images recorded using a transmission electron microscope (TEM) for (a) cotton-extracted cellulose, (b) nanocrystalline cellulose, (c) chemical TiO_2 , (d) green synthesized TiO_2 , (e) CNC (NCell: C- TiO_2 nanocomposite) and (f) GNC (NCell: G- TiO_2 nanocomposite).

Table 2 The hydrodynamic size of particles of all the samples, along with their PDI value obtained by DLS analysis

Sample	Hydrodynamic size (nm)	PDI value
NCell	78.8	0.584
C- TiO_2	58.8	0.9
G- TiO_2	58.8	0.4
CNC	37.8	0.327
GNC	21	0.2

is not enough to be defensive against the pathogens. Thus, the 4 mg ml^{-1} concentration is found to be the optimized reactive concentration against pathogen Xcc, so the results obtained from this concentration are presented here to be analyzed.

The obtained results manifest that the chemical TiO_2 (C- TiO_2) nanoparticles have shown an inhibition zone (IZ) of 10 mm until 24 h, and beyond that, bacterial growth was observed inside the IZ. Thus, Fig. 5 depicts no activity of C- TiO_2 NPs against Xcc, while green synthesized TiO_2 depicts a 20 mm clear inhibition zone (IZ) up to 48 h. This suggests that the phytochemicals present in neem extract played a role in the



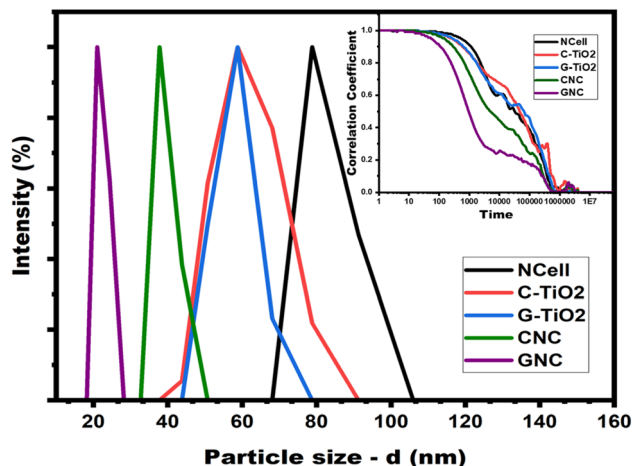


Fig. 4 DLS spectra showing the particle size distribution of (a) nanocrystalline cellulose (NCell), (b) chemical TiO₂ (C-TiO₂), (c) green synthesized TiO₂ (G-TiO₂), (d) CNC (NCell : C-TiO₂ nanocomposite) and (e) GNC (NCell : G-TiO₂ nanocomposite); inset showing the correlation coefficient versus time plot of all the samples.

bacterium. However, the G-TiO₂ NPs could no longer resist the pathogen attack, and bacterial cells could even cover the inhibition zone after 48 h. Similarly, the nanocrystalline cellulose (NCell) extracted from cotton cloth also showed an 18 mm IZ until 48 h and depicted bacteriostatic activity (NPs still resist bacterial growth with a 1 mm clear IZ) against Xcc after 72 h. However, the nanocomposites (CNC and GNC) showed promising results even after 72 h. The nanocomposite (CNC) of NCell and chemically synthesized TiO₂ manifests a 30 mm IZ up to 48 h and even beyond that showed a 24 mm IZ up to 72 h, whereas the nanocomposite (GNC) of NCell and green synthesized TiO₂ demonstrated a 44 mm IZ even after 72 h. It significantly involves the action of phytochemicals associated with neem (*Azadirachta indica*). Firstly, the neem extract acts as a capping agent responsible for particle size reduction. Secondly, the phytochemicals present in neem also played defensive roles against pathogens, either by weakening the bacterial cell wall or slowing cell growth. The reactivity of GNC

against Xcc up to 72 h evidences the synergistic effect of NCell and G-TiO₂ NPs as well as the strong defensive role of phytochemical-rich neem extract against phytopathogen.

It is necessary to investigate that the nanomaterial showing activity against phytopathogens should not harm plant health. Thus, all the synthesized nanomaterials tested against pathogens *Bacillus subtilis* (BS) and *Pseudomonas fluorescens* (PSFL) are biocontrol agents maintaining plant health. The results shown in Fig. 6a manifest the activity of nanomaterials against the biocontrol *B. subtilis* (BS). Green synthesized TiO₂ and its corresponding nanocomposite (GNC) inhibited the bacterial growth until 48 h with an 8 mm and a 20 mm IZ, respectively. In spite of this, the nanomaterials (G-TiO₂ and GNC) could no longer resist bacterial growth beyond 48 h and became ineffective against pathogen BS. On the other hand, Fig. 6b also depicts similar results that *P. fluorescens* growth was inhibited by green synthesized TiO₂ (GNC) with a 6 mm IZ until 48 h, but these NPs could not be effective for another 24 h (no IZ after 72 h). This suggests that the nanomaterials which showed activity against phytopathogens Xcc are not harmful against biocontrol agents BS and PSFL. The measurement of the inhibition zone observed from antibacterial testing of all the nanomaterials against phytopathogens is noted in Table 3, which indicates the potential of the prepared nanocomposites.

3.5 The defense mechanism of nanomaterials against pathogens

The obtained antibacterial results were analyzed based on the observed inhibition zone. Fig. 7 attempts to explain the scenario inside the inhibition zone, or the defence mechanism of the material against pathogens, using TEM images of untreated Xcc and treated Xcc by the G-TiO₂ nanomaterial as an example. In this respect, a very small area inside the inhibition zone of the G-TiO₂ plate (72 h) was swept out, dispersed in autoclaved DI water, and further used to prepare the TEM grid for testing. It is seen from Fig. 7 that the untreated bacterium is a rod-shaped microorganism with a fine thick cell wall and thread-like flagella. On the other hand, there are two types of defensive action during a pathogen treatment with a nanomaterial:

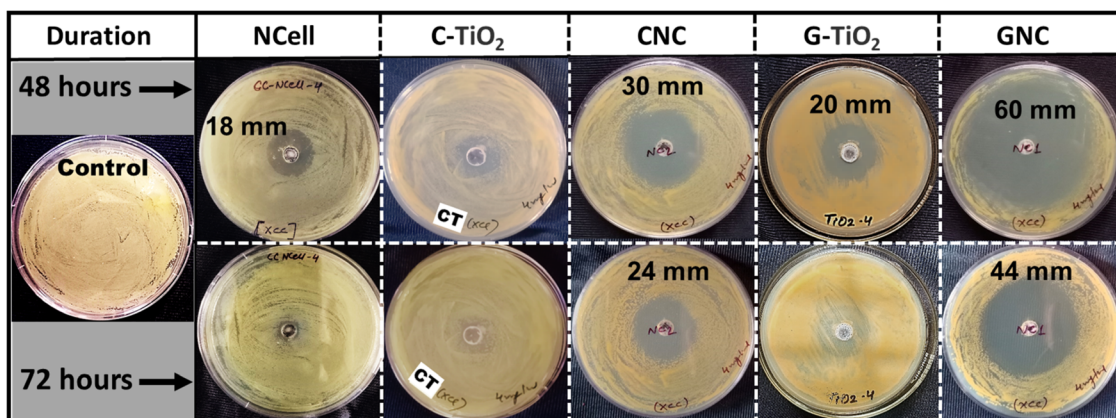


Fig. 5 Antibacterial activity of synthesized nanomaterials at a 4 mg ml⁻¹ concentration against phytopathogen *X. campestris* pv. *campestris*.

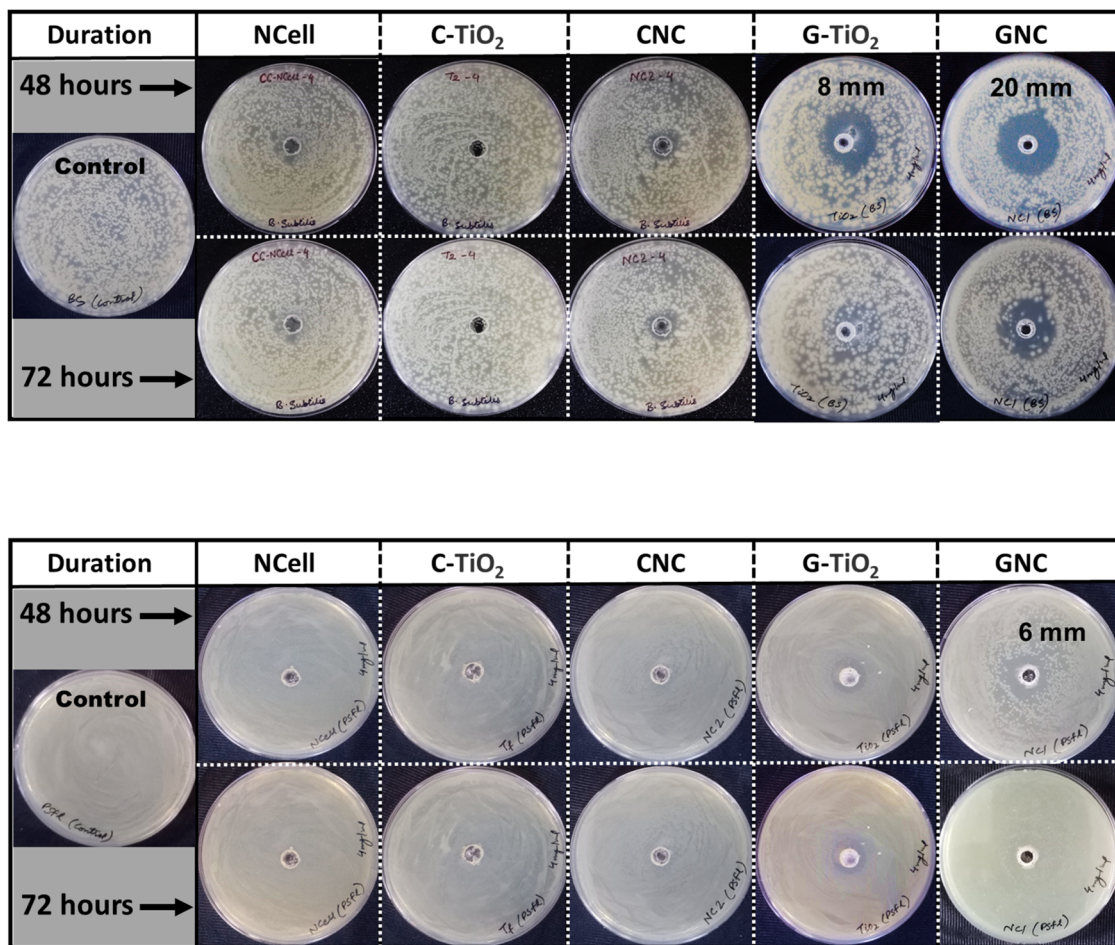


Fig. 6 (a) Agar well diffusion assay testing of nanomaterials at a 4 mg ml⁻¹ concentration against biocontrol agent *Bacillus subtilis* (BS). (b) Agar well diffusion assay testing of nanomaterials at a 4 mg ml⁻¹ concentration against biocontrol agent *Pseudomonas fluorescens* (PSFL).

Table 3 Measurement of the inhibition zone observed from anti-bacterial testing of nanomaterials against phytopathogens. NI represents no inhibition

Materials	Zone of inhibition (mm)					
	Xcc		BS		PSFL	
	48 h	72 h	48 h	72 h	48 h	72 h
NCell	18	NI	NI	NI	NI	NI
C-TiO ₂	NI	NI	NI	NI	NI	NI
G-TiO ₂	20	NI	8	NI	NI	NI
CNC	30	24	NI	NI	NI	NI
GNC	60	44	20	NI	6	NI

bactericidal and bacteriostatic. In this example case, G-TiO₂ showed bactericidal action until 48 h showing a clear inhibition zone. This means the nanoparticles could successfully rupture the bacterial cell wall and penetrate the cell to kill it. However, after 48 h, the strength of nanoparticles decreases with further bacterial growth. Although, at this stage (after 48 h), G-TiO₂ NPs could not penetrate the bacterial cell, they are still effective enough to weaken or inactivate the bacterium making it

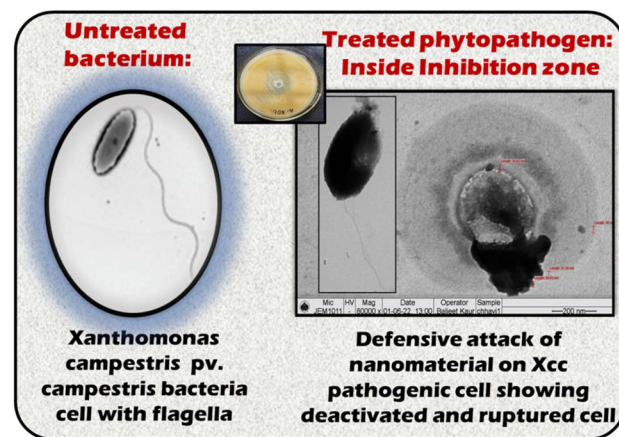


Fig. 7 Schematic of TEM images depicting the action on green synthesized TiO₂ on phytopathogen *X. campestris* pv. *campestris* (Xcc).

unconscious. It basically suppresses the growth of bacterial cells, keeping them in a stationary phase of growth known as a bacteriostatic condition. Thus, the TEM images recorded for

the sample inside the inhibition zone of the 72 h condition of the G-TiO₂ sample plate show dead cells with ruptured cell walls and deactivated cells, also depicting bacteriostatic conditions.

3.6 Antifungal studies of synthesized nanomaterials

The antifungal activity of prepared nanocomposites in comparison with their parent components was analyzed using poison food agar assay against pathogens *Fusarium graminearum* and *Phytophthora* spp., and the results are presented in Fig. 8. Since the antibacterial studies revealed 4 mg ml⁻¹ to be the optimized concentration, this concentration is considered a reference for antifungal studies. However, it was found that all the nanomaterials at 4, 2, 1, and 0.5 mg ml⁻¹ concentrations exhibited the complete inhibition of mycopathogens *Fusarium g.* and *Phytophthora* spp. even after 7 days, and the control plate showed full fungus growth within 5 days. Thus, the nanomaterial concentration was further lowered to find the minimum optimized concentration effective against fungus. Fig. 8a shows the antifungal results of nanomaterials at 0.25 and 0.125 mg ml⁻¹ concentrations against *Fusarium graminearum* (FG). It has been found that the 0.25 mg ml⁻¹ concentration is strongly effective against FG as all the nanomaterials completely inhibit the fungal growth. However, the results at the 0.125 mg ml⁻¹ concentration are quite different, but the nanomaterials are still effective against FG as they showed restricted growth compared with the control plate. Moreover, the PDA plate consisting of G-TiO₂ showed no fungal growth, while only the plug of 3-day mycelial growth placed in the PDA plate of GNC is covered with fungus FG and could not grow

beyond due to the defensive action of GNC NPs. Thus, this suggests that the green synthesized TiO₂ and its corresponding nanocomposite completely inhibit the fungal growth even at 0.125 mg ml⁻¹ concentration and thus prove their potential for preventing FHB diseases caused by *F. graminearum* in wheat and barley.

However, all the nanomaterials exhibited strong inhibition of fungal growth of *Phytophthora* spp. even at 0.125 mg ml⁻¹ concentration, as shown in Fig. 8b. It can be seen that the control plate showed full fungal growth within 5 days while all the nanomaterials exhibited complete inhibition and thus are strongly effective against *Phytophthora* spp. This suggests that all the prepared nanomaterials have the ability to control water and soil-borne diseases caused by *Phytophthora* spp. in citrus.

Thus, the obtained antimicrobial results manifest that the synergistic effects of nanocrystalline cellulose and TiO₂ are stronger than those of the individual nanomaterials. Moreover, the *Azadirachta indica* leaf extract contributed well to the defense mechanism against pathogens. The phytochemicals in green extract acted as a reducing agent during synthesis and as a capping agent to stop further growth and maintain smaller particle sizes. So, the phytochemicals help weaken the bacterial cell wall so that smaller-sized particles^{61,62} easily penetrate the cytoplasm by damaging the cell wall and rupturing the membrane, causing vacuole formation due to increased NP concentration in the cell, inhibiting cell growth, and finally opening the death pathways for pathogens either by deactivating or killing the bacteria. Hence, the nanocomposite of cotton cloth extracted nanocrystalline cellulose with green synthesized

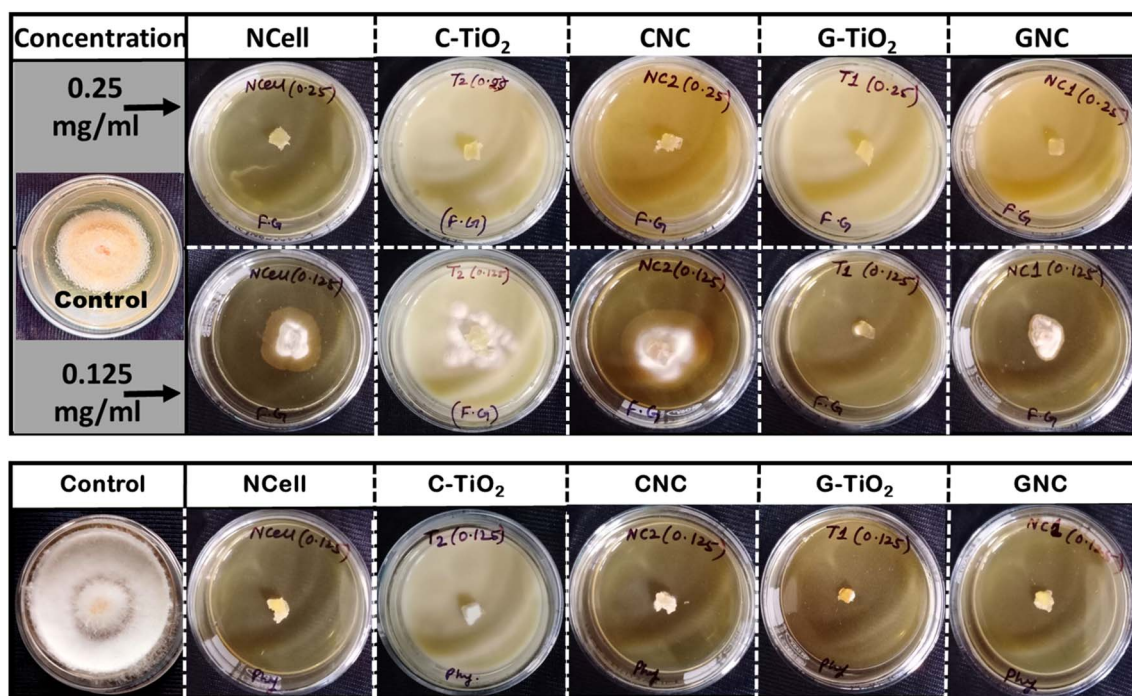


Fig. 8 (a) Poison food agar assay testing of all the nanomaterials at 0.25 and 0.125 mg ml⁻¹ concentrations against *F. graminearum* under *in vitro* conditions. (b) Poison food agar assay testing of all the nanomaterials at a 0.125 mg ml⁻¹ concentration against *Phytophthora* spp. under *in vitro* conditions.

TiO₂ has proved its potential to be a good antimicrobial agent for crop protection in agriculture.

4. Conclusions

This work presents two different non-toxic, biocompatible compounds to prepare environmentally friendly nanocomposites. A waste product (waste cotton cloth) has been recycled successfully used to prepare cellulose nanoparticles and tested against pathogens. Another biocompatible compound TiO₂ has been green synthesized by using *Azadirachta indica* leaf extract to utilize the effects of phytochemicals against pathogens. Moreover, commercially available TiO₂ has also been used for comparison. So, two nanocomposites of nanocrystalline cellulose (NCell) have been prepared, one with chemical TiO₂ and another with green TiO₂. All the nanomaterials (NCell, C-TiO₂, G-TiO₂, CNC and GNC) were analysed by XRD, UV-visible spectroscopy and TEM. The results obtained from XRD and UV-visible spectroscopy evidence the contribution of NCell and TiO₂ in nanocomposites. The TEM results demonstrate the particle size of nanomaterials and prove that GNC particle size is smaller than that of CNC. The prepared nanocomposites, in comparison with individual parent components, have been examined against phytopathogens: *Xanthomonas campestris* pv. *campestris* and two biocontrol agents – *Bacillus subtilis* and *Pseudomonas fluorescens*; fungal pathogens: *Fusarium graminearum* and *Phytophthora* spp. It is evident from the antibacterial results against Xcc that only the nanocomposites CNC and GNC showed bactericidal action even after 72 h with an inhibition zone of 24 and 44 mm, respectively. However, comparing CNC and GNC with each other, the phytochemicals present in the green extract are responsible for stronger and longer defensive actions of the GNC nanocomposite against Xcc compared to CNC. Similarly, the nanocomposites have proved their efficiency against fungi *F. graminearum* and *Phytophthora* spp. Moreover, all the prepared nanomaterials have not affected the growth of *B. subtilis* and *P. fluorescens*, which are biocontrol agents helping to maintain plant health. Thus, the results evidently demonstrated that the nanocomposites exhibited enhanced antimicrobial activity compared to their individual components, with the green-synthesized TiO₂ showing superior performance. This enhanced efficacy is attributed to the synergistic effects of TiO₂ and cellulose, which disrupt bacterial and fungal cell walls more effectively. The nanocomposites also displayed excellent biocompatibility, ensuring that they do not harm beneficial microbes. The green synthesis method further reduced particle agglomeration, improved stability, and minimized environmental impact, aligning with sustainability principles. This approach highlights the potential of waste-derived nanomaterials in sustainable agriculture. Using cellulose extracted from waste cotton cloth not only reduces waste but also creates value-added products for agricultural applications. Similarly, green synthesis using neem extract leverages natural resources to produce environmentally friendly nanoparticles without hazardous chemicals. Thus, the present study demonstrates that nanocomposites of cellulose and TiO₂, particularly those

synthesized using green methods, offer a promising solution for managing plant diseases. These materials provide effective antimicrobial action against harmful pathogens while preserving beneficial biocontrol agents. Their cost-effectiveness, environmental safety, and scalability make them suitable for widespread agricultural use. By integrating advanced nanotechnology with sustainable practices, this work contributes to improving crop protection and ensuring global food security.

Data availability statement

The raw/processed data required to reproduce the above findings cannot be shared at this time due to legal/ethical reasons.

Author contributions

Chhavi Sharma: conceptualization, original draft, methodology, investigation, data curation, and experimentation. Archana Rana and Amit Kumar Kesharwani: resources and software. Dinesh Singh: supervision for antimicrobial testing and analysis. Ritu Srivastava: co-supervision & editing. Shailesh Narain Sharma: supervision; validation; visualization; review & editing.

Conflicts of interest

The authors declare that they have no known competing financial interests or personal relationships that could have appeared to influence the work reported in this paper.

Acknowledgements

The authors express gratitude to Director CSIR-NPL for permitting them to utilize facilities to execute the research work. C. Sharma sincerely acknowledges the Academy of Scientific and Innovative Research (AcSIR) to pursue a PhD at CSIR-NPL.

References

- 1 S. Savary, L. Willocquet, S. J. Pethybridge, P. Esker, N. McRoberts and A. Nelson, *Nat. Ecol. Evol.*, 2019, **3**, 430–439.
- 2 X.-F. Xin, B. Kvitko and S. Y. He, *Nat. Rev. Microbiol.*, 2018, **16**, 316–328.
- 3 L. Perincherry, J. Lalak-Kańczugowska and Ł. Stępień, *Toxins*, 2019, **11**, 664.
- 4 M. J. Hajipour, K. M. Fromm, A. Akbar Ashkarran, D. Jimenez de Aberasturi, I. R. de Larramendi, T. Rojo, V. Serpooshan, W. J. Parak and M. Mahmoudi, *Trends Biotechnol.*, 2012, **30**, 499–511.
- 5 N.-Y. T. Nguyen, N. Grelling, C. L. Wetteland, R. Rosario and H. Liu, *Sci. Rep.*, 2018, **8**, 16260.
- 6 L. Miao, C. Wang, J. Hou, P. Wang, Y. Ao, Y. Li, N. Geng, Y. Yao, B. Lv, Y. Yang, G. You and Y. Xu, *Bioresour. Technol.*, 2016, **216**, 537–544.



- 7 C. López de Dicastillo, M. Guerrero Correa, F. B. Martínez, C. Streitt and M. José Galotto, in *Antimicrobial Resistance – A One Health Perspective*, ed. M. Mareş, S. Hua Erin Lim, K.-S. Lai and R.-T. Cristina, IntechOpen, 2021.
- 8 Y. He, S. Ingudam, S. Reed, A. Gehring, T. P. Strobaugh and P. Irwin, *J. Nanobiotechnol.*, 2016, **14**, 54.
- 9 J. Chen, H. Peng, X. Wang, F. Shao, Z. Yuan and H. Han, *Nanoscale*, 2014, **6**, 1879–1889.
- 10 S. Shamaila, N. Zafar, S. Riaz, R. Sharif, J. Nazir and S. Naseem, *Nanomaterials*, 2016, **6**, 71.
- 11 K. Markowska, A. M. Grudniak and K. I. Wolska, *Acta Biochim. Pol.*, 2013, **60**, 523–530.
- 12 J. Chen, L. Wu, M. Lu, S. Lu, Z. Li and W. Ding, *Front. Microbiol.*, 2020, **11**, 365.
- 13 J. Pečenka, Z. Bytešniková, T. Kiss, E. Peňázová, M. Baránek, A. Eichmeier, D. Tekielska, L. Richtera, R. Pokluda and V. Adam, *Mater. Today Commun.*, 2021, **27**, 102284.
- 14 B. Thomas, M. C. Raj, A. K. B., R. M. H., J. Joy, A. Moores, G. L. Drisko and C. Sanchez, *Chem. Rev.*, 2018, **118**, 11575–11625.
- 15 K. Heise, E. Kontturi, Y. Allahverdiyeva, T. Tammelin, M. B. Linder, Nonappa and O. Ikkala, *Adv. Mater.*, 2021, **33**, 2004349.
- 16 K. J. Edgar, C. M. Buchanan, J. S. Debenham, P. A. Rundquist, B. D. Seiler, M. C. Shelton and D. Tindall, *Prog. Polym. Sci.*, 2001, **26**, 1605–1688.
- 17 M. Rose and R. Palkovits, *Macromol. Rapid Commun.*, 2011, **32**, 1299–1311.
- 18 S. Kalia, A. Dufresne, B. M. Cherian, B. S. Kaith, L. Avérous, J. Njuguna and E. Nassiopoulou, *Int. J. Polym. Sci.*, 2011, **2011**, 1–35.
- 19 I. Siró and D. Plackett, *Cellulose*, 2010, **17**, 459–494.
- 20 S. Ummartyotin and C. Pechyen, *Carbohydr. Polym.*, 2016, **142**, 133–140.
- 21 L. Zheng, S. Li, J. Luo and X. Wang, *Front. Bioeng. Biotechnol.*, 2020, **8**, 593768.
- 22 R. Koshani, J. Zhang, T. G. M. van de Ven, X. Lu and Y. Wang, *ACS Sustain. Chem. Eng.*, 2021, **9**, 10513–10523.
- 23 D. Georgouvelas, H. N. Abdelhamid, J. Li, U. Edlund and A. P. Mathew, *Carbohydr. Polym.*, 2021, **264**, 118044.
- 24 V. A. Spirescu, C. Chircov, A. M. Grumezescu, B. Ștefan Vasile and E. Andronescu, *Int. J. Mol. Sci.*, 2021, **22**, 4595.
- 25 V. Rodríguez-González, C. Terashima and A. Fujishima, *J. Photochem. Photobiol., C*, 2019, **40**, 49–67.
- 26 X.-X. Chen, B. Cheng, Y.-X. Yang, A. Cao, J.-H. Liu, L.-J. Du, Y. Liu, Y. Zhao and H. Wang, *Small*, 2013, **9**, 1765–1774.
- 27 K. P. Priyanka, T. H. Sukirtha, K. M. Balakrishna and T. Varghese, *IET Nanobiotechnol.*, 2016, **10**, 81–86.
- 28 B. Kim, D. Kim, D. Cho and S. Cho, *Chemosphere*, 2003, **52**, 277–281.
- 29 J.-W. Liou and H.-H. Chang, *Arch. Immunol. Ther. Exp.*, 2012, **60**, 267–275.
- 30 H. A. Foster, I. B. Ditta, S. Varghese and A. Steele, *Appl. Microbiol. Biotechnol.*, 2011, **90**, 1847–1868.
- 31 M. R. Khan and Z. A. Siddiqui, *Gesunde Pflanz.*, 2021, **73**, 445–464.
- 32 Q. Zhang, X. Yan, R. Shao, H. Dai and S. Li, *J. Wuhan Univ. Technol., Mater. Sci. Ed.*, 2014, **29**, 407–409.
- 33 M. A. Irshad, R. Nawaz, M. Zia ur Rehman, M. Imran, J. Ahmad, S. Ahmad, A. Inam, A. Razzaq, M. Rizwan and S. Ali, *Chemosphere*, 2020, **258**, 127352.
- 34 B. K. Thakur, A. Kumar and D. Kumar, *S. Afr. J. Bot.*, 2019, **124**, 223–227.
- 35 A. K. Kesharwani, D. Singh, A. Kulshreshtha, A. S. Kashyap, A. S. Avasthi and N. Geat, *Plant Dis.*, 2023, **107**, 212.
- 36 D. Singh, P. S. Rathaur and J. G. Vicente, *Plant Pathol.*, 2016, **65**, 1411–1418.
- 37 D. Singh, A. K. Kesharwani, K. Singh, S. Jaiswal, M. A. Iquebal, N. Geat and A. S. Avasthi, *Plant Dis.*, 2022, **106**, 1502–1505.
- 38 S. Sreelatha, N. Kumar and S. Rajani, *Front. Microbiol.*, 2022, **13**, 1085113.
- 39 A. Varympopi, A. Dimopoulou, I. Theologidis, T. Karamanidou, A. Kaldeli Kerou, A. Vlachou, D. Karfaridis, D. Papafotis, D. G. Hatzinikolaou, A. Tsouknidas and N. Skandalis, *Pathogens*, 2020, **9**, 1024.
- 40 H. Peng and I. A. Chen, *ACS Nano*, 2019, **13**(2), 1244–1252.
- 41 S. Malmir, A. Karbalaei, M. Pourmadadi, J. Hamed, F. Yazdian and M. Navae, *Carbohydr. Polym.*, 2020, **234**, 115835.
- 42 M. K. Khan, A. Pandey, T. Athar, S. Choudhary, R. Deval, S. Gezzin, M. Hamurcu, A. Topal, E. Atmaca, P. A. Santos, M. R. Omay, H. Suslu, K. Gulcan, M. Inanc, M. S. Akkaya, A. Kahraman and G. Thomas, *3 Biotech*, 2020, **10**, 172.
- 43 M. McMullen, G. Bergstrom, E. De Wolf, R. Dill-Macky, D. Hershman, G. Shaner and D. Van Sanford, *Plant Dis.*, 2012, **96**, 1712–1728.
- 44 J. Graham and E. Feichtenberger, *J. Citrus Pathol.*, 2015, **2**(1), DOI: [10.5070/C421027203](https://doi.org/10.5070/C421027203).
- 45 S. O. Cacciola and G. M. D. S. Lio, in *Integrated Management of Diseases Caused by Fungi, Phytoplasma and Bacteria*, ed. A. Ciancio and K. G. Mukerji, Springer Netherlands, Dordrecht, 2008, pp. 61–84.
- 46 D. Singh, D. K. Yadav, S. Sinha, K. K. Mondal, G. Singh, R. R. Pandey and R. Singh, *Afr. J. Microbiol. Res.*, 2013, **7**, 5459–5470.
- 47 T. Stein, *Mol. Microbiol.*, 2005, **56**, 845–857.
- 48 G. Ganeshan and A. Manoj Kumar, *J. Plant Interact.*, 2005, **1**, 123–134.
- 49 C. Sharma, S. N. Sharma and R. Srivastava, *Colloid Polym. Sci.*, 2022, **300**, 1027–1036.
- 50 A. H. Bashal, K. D. Khalil, A. M. Abu-Dief and M. A. El-Atawy, *Int. J. Biol. Macromol.*, 2023, **253**, 126856.
- 51 A. M. Abu-Dief, F. M. M. Alrashedee, K. M. Emran and H. A. Al-Abdulkarim, *Inorg. Chem. Commun.*, 2022, **138**, 109251.
- 52 Ž. Antić, R. M. Krsmanović, M. G. Nikolić, M. Marinović-Cincović, M. Mitrić, S. Polizzi and M. D. Dramićanin, *Mater. Chem. Phys.*, 2012, **135**, 1064–1069.
- 53 A. D. French, *Cellulose*, 2014, **21**, 885–896.
- 54 D. Bondeson, A. Mathew and K. Oksman, *Cellulose*, 2006, **13**, 171–180.



- 55 J. Gong, J. Li, J. Xu, Z. Xiang and L. Mo, *RSC Adv.*, 2017, **7**, 33486–33493.
- 56 E. M. M. Ibrahim, A. M. Abu-Dief, A. Elshafaie and A. M. Ahmed, *Mater. Chem. Phys.*, 2017, **192**, 41–47.
- 57 L. H. Abdel Rahman, A. M. Abu-Dief, R. M. El-Khatib, S. M. Abdel-Fatah, A. M. Adam and E. M. M. Ibrahim, *Appl. Organomet. Chem.*, 2018, **32**, e4174.
- 58 T. T. Win, S. Khan and P. Fu, *J. Nanotechnol.*, 2020, **2020**, 1–9.
- 59 A. K. Madbouly, M. S. Abdel-Aziz and M. A. Abdel-Wahhab, *IET Nanobiotechnol.*, 2017, **11**, 702–708.
- 60 M. AlMatar, E. A. Makky, I. Var and F. Koksai, *Curr. Drug Delivery*, 2018, **15**, 470–484.
- 61 C. Lee, J. Y. Kim, W. I. Lee, K. L. Nelson, J. Yoon and D. L. Sedlak, *Environ. Sci. Technol.*, 2008, **42**, 4927–4933.
- 62 J. Yu, W. Zhang, Y. Li, G. Wang, L. Yang, J. Jin, Q. Chen and M. Huang, *Biomed. Mater.*, 2014, **10**, 015001.

